Supporting Information:

Towards highly conducting bicarbazole redox polymer films with plateau-like conductivities

Claudia Malacrida,[1] Yushi Lu[1], Klaus Dirnberger[1], Sergio Gámez-Valenzuela[2], M. Carmen Ruiz Delgado[2], Sabine Ludwigs[1]*

[1] IPOC-Functional Polymers, Institute of Polymer Chemistry, University of Stuttgart, Pfaffenwaldring 55, 70569 Stuttgart, Germany

[2] Department of Physical Chemistry, University of Málaga, 29071 Málaga, Spain

Corresponding author: sabine.ludwigs@ipoc.uni-stuttgart.de

1. Polymers

PVTPA: To a stirred solution of N,N-diphenyl-4-vinylaniline[1] (4.73 g, 14.43 mmol, 1 eq.) in freshly distilled THF, AIBN (57.24 mg, 0.3486 mmol, 0.02 eq.) was added. The reaction mixture was then heated to 50°C for 15 hours. The polymer was precipitated from cold acetone and reprecipitated from THF/acetone[1] to obtain 1.8 g of white powder. Size exclusion chromatography (SEC) vs. polystyrene (PS) standards (THF, 30°C): M_n= 29 000 g/mol; M_w = 48 000 g/mol; PDI = 1.6. Synthesis was adapted from ref 1.

PVPhCbz: To a stirred solution of 9-(4-Vinylphenyl)-9H-carbazole (500 mg, 1.86 mmol, 1 eq.) in freshly distilled toluene (freeze-pump-thaw degassed 3 times) AIBN was added (freshly recrystallized from MeOH) (10 mg, 0.02 mmol, 0.01 eq.). The reaction mixture was then heated to 70°C for 12 hours. The polymer was precipitated from cold methanol; 300 mg of raw product are obtained. The polymer is dissolved in THF and filtered using disposable syringe filters with a pore size of 0.45 µm; 150 mg of polymer are finally obtained. SEC vs. PS standards (THF, 30°C): M_n= 2 260 g/mol; M_w = 3 900 g/mol; PDI = 1.7. Reaction was adapted from references 1–4.

PVCbz: PVCbz was purchased from Sigma Aldrich and used as received. SEC vs. PS standards (THF, 30°C): M_n= 19 400 g/mol; M_w = 64 300 g/mol; PDI = 3.3.

References:
1. M. Behl, E. Hattemer, M. Brehmer, R. Zentel, *Macromol. Chem. Phys.* 2002, *203*, 503–510.
2. N. B. McKeown, S. Badriya, M. Helliwell, M. Shkunov, *J. Mater. Chem.* 2007, *17*, 2088–2094.
3. F. Monnier, M. Taillefer, *Angew. Chemie* 2009, *121*, 7088–7105..
4. H. P. Shi, L. Xu, Y. Cheng, J. Y. He, J. X. Dai, L. W. Xing, B. Q. Chen, L. Fang, *Spectrochim. Acta - Part A Mol. Biomol. Spectrosc.* 2011, *81*, 730–738.

2. Chemical doping with $FeCl_3$

All chemical doping experiments presented in the manuscript were performed in a nitrogen filled glove-box to allow for a reliable comparison between conductivities and related absorption spectra.

Figure S 1 shows the development of a sequentially doped PVTPA film (4 mg/mL solution for 60 s). The film was then exposed to air and UV-Vis-NIR absorption spectra and electronic conductivities were measured every 10 min in order to follow their variation in correlation to air exposure time.

We found that upon contact with air the film absorption progressively changes, as the dication band with maximum at 804 nm bleaches with concomitant increase in intensity of the characteristic radical cation band with maximum at 479 nm. After 60 min of air exposure, a coexistence of radical cation and dication species becomes visible and stable. While the starting conductivity is low, after 60 min conductivity values as high as $2 \cdot 10^{-3}$ S/cm are reached which are comparable to the highest conductivities for samples measured in the glovebox when exposed to 2 mg/ml $FeCl_3/CH_3CN$ for 10 s.

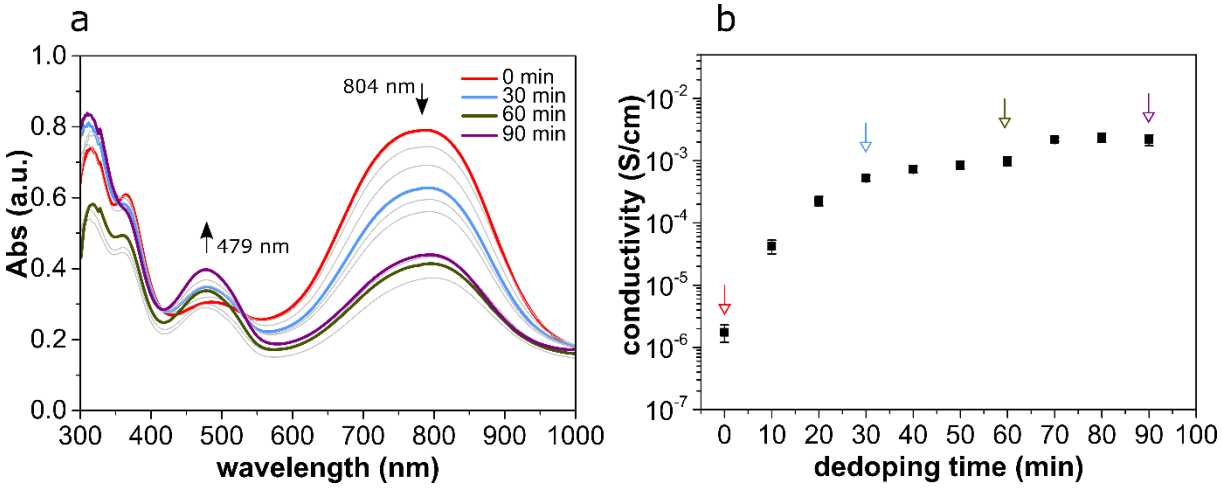

Figure S 1: *Development of a doped PVTPA film (doped with 4 mg/mL $FeCl_3/CH_3CN$ for 1 min) at time 0 min, when exposed to air. De-doping in air is followed by UV-Vis (a) and additionally conductivity measurements were performed (b).*

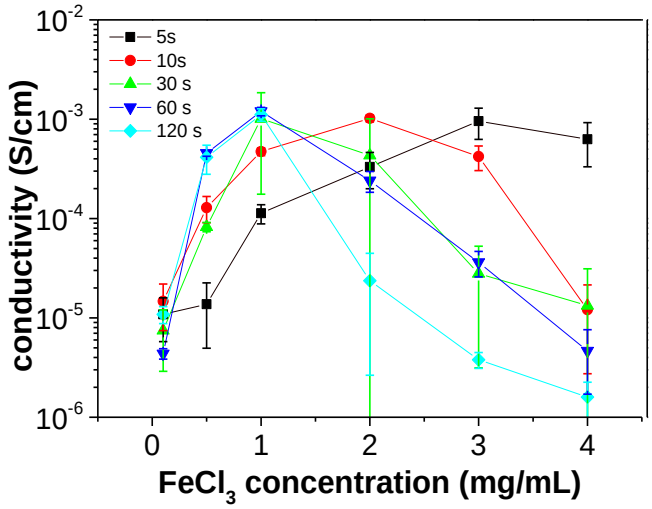

Figure S 2: *Sequential doping of a PVTPA film with $FeCl_3/CH_3CN$ solutions with different concentrations (0.1; 0.5; 1; 2; 3 and 4 mg/mL) and for different doping times.*

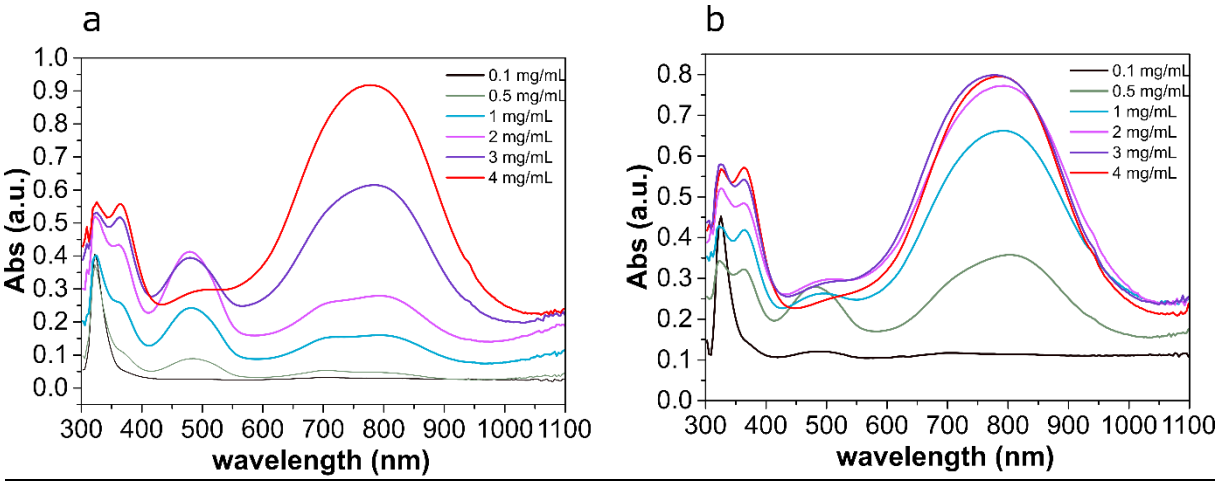

Figure S 3: UV-Vis-NIR of sequentially doped PVTPA films with $FeCl_3/CH_3CN$ for (a) 10 s and (b) 60 s. The correlated conductivity data are presented in Figure 1 of the main manuscript (10 s) and Figure S 2 (60 s).

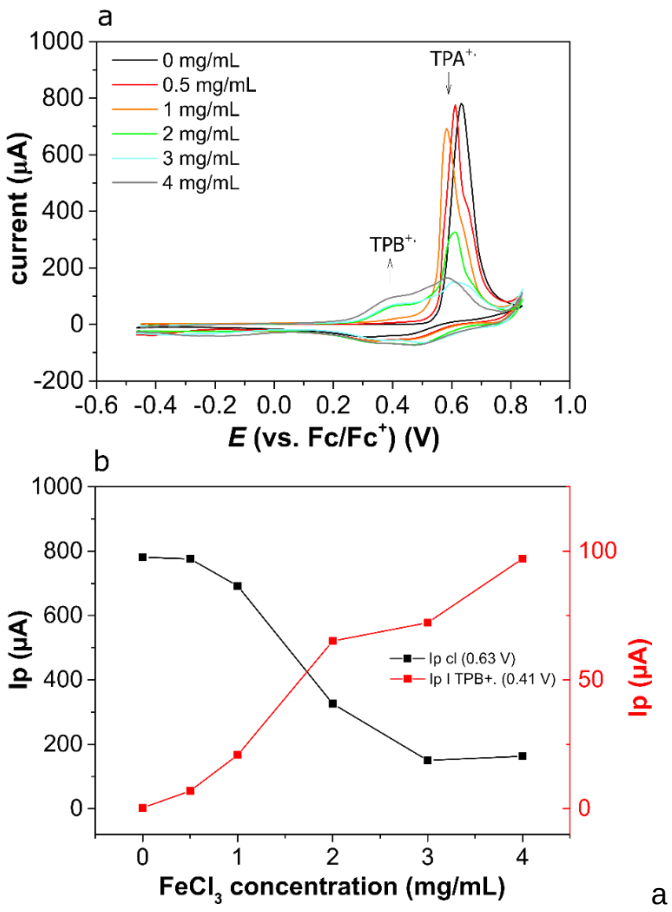

Figure S 4: Post-electrochemical characterization of sequentially doped PVTPA films. a) CV of chemically oxidized samples (after 10s $FeCl_3/CH_3CN$ at different concentrations indicated) in $CH_3CN/n\text{-}NBu_4PF_6$ (0.1 M) at 20 mV/s. The first cycle is shown to visualize remaining non-crosslinked TPA units still present in the films. b) Extracted peak current variation from the CV in a) for the first forward CV cycle for the cross-linking peak at 0.63 V and the first oxidation of TPB units at 0.41 V.

With increasing the oxidant concentration the intensity of the crosslinking peak (0.64 V) progressively decreases whereas the $TPB^{+\bullet}$ peak current increases. Additionally, also in the case of the low conducting 4 mg/mL oxidized sample, the $TPA^{+\bullet}$ peak in the voltammetric

experiment can still be observed. The presence of un-dimerized neutral monomers, even when the majority of the film is in its dication state, can be explained by the lower oxidation potential of the dimeric species for oxidation with respect to the monomer, resulting in their favoured oxidation with respect to new dimerization.

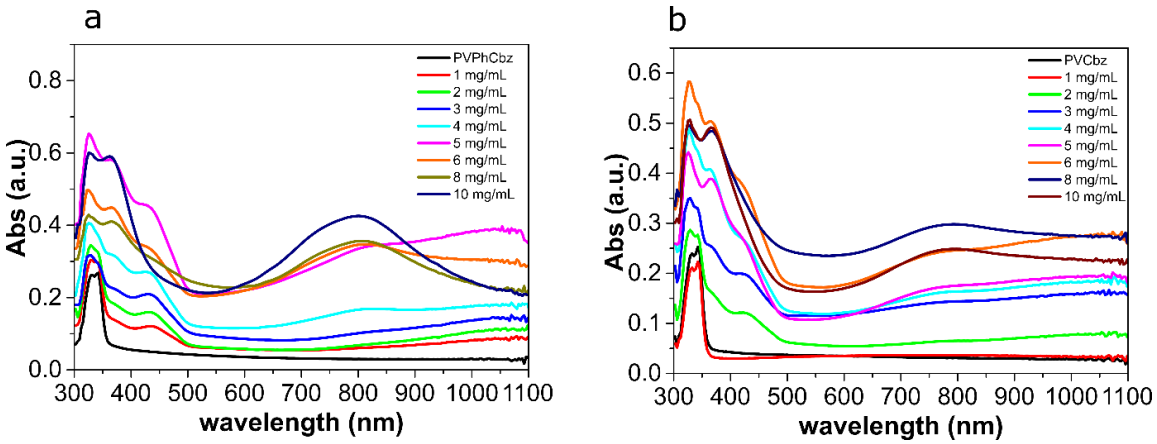

Figure S 5: *UV-Vis of sequentially doped films of PVPhCbz in a) and PVCbz in b) with $FeCl_3/CH_3CN$ for 10 s. The correlated conductivity data are presented in Figure 1 of the main manuscript.*

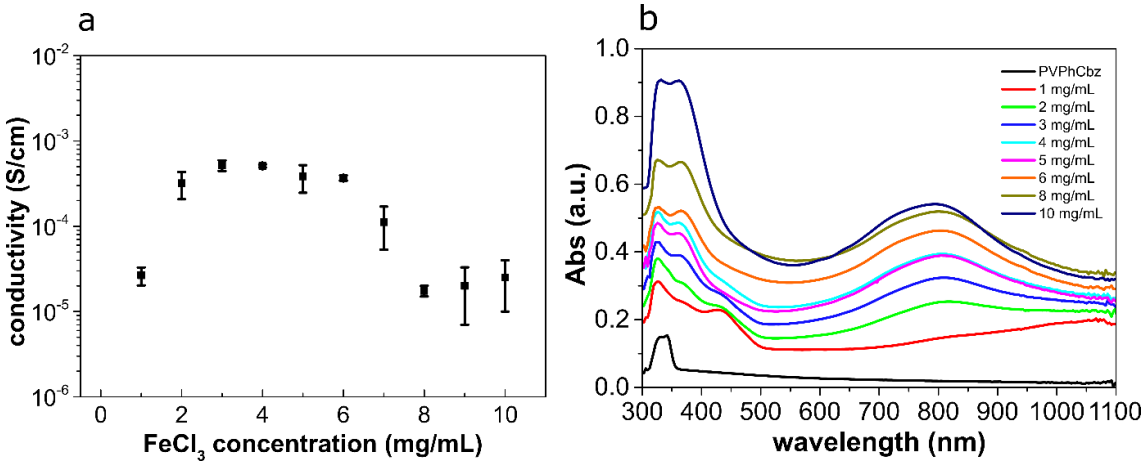

Figure S 6: Chemical crosslinking and doping of PVPhCbz films with $FeCl_3/CH_3CN$ for 60 s exposure time. (a) Electronic conductivity and (b) corresponding UV-Vis absorption spectra.

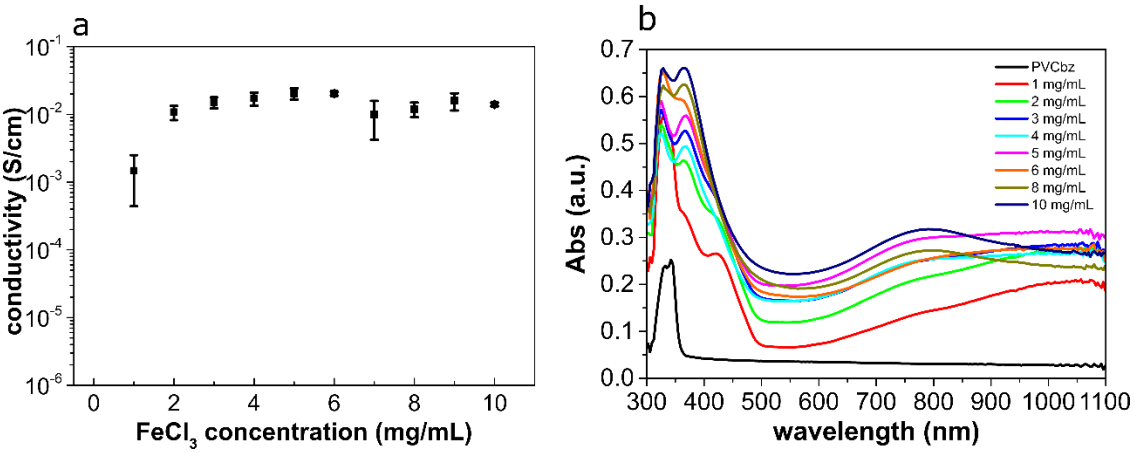

Figure S 7: *Sequential doping of PVCbz films with $FeCl_3/CH_3CN$ for 60 s exposure with different concentrations. (a) Electronic conductivity and (b) corresponding UV-Vis absorption spectra.*

3. Model experiments with N-ethylcarbazole

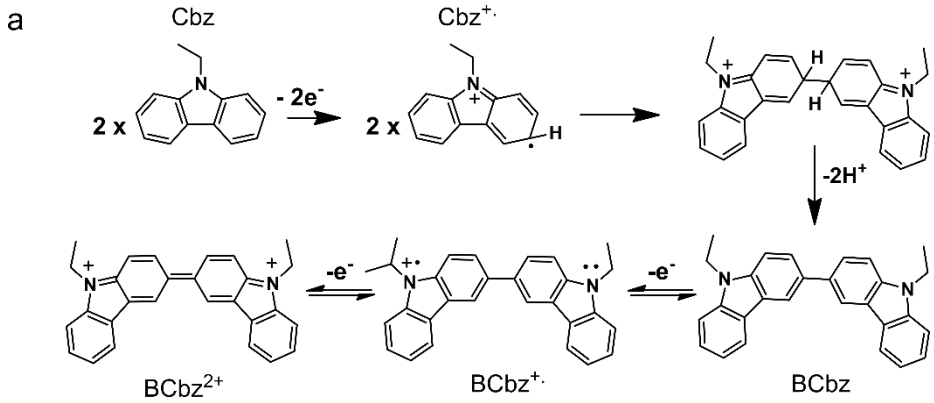

Figure S 8: Dimerization mechanism of N-ethylcarbazole upon oxidation: Carbazole oxidation to radical cation, coupling of two radical cations, proton elimination of charged dimer (BCbz). Dimer can undergo reversible oxidation to the radical cation and dication state in two subsequent one electron oxidations.

The electrolysis of N-ethylcarbazole was conducted with similar conditions with respect to the voltammetric experiment of the polymer. A 2.5 mM solution of N-ethylcarbazole dissolved in the electrolyte solution, CH_3CN/Bu_4NPF_6 0.1 M, was potentiostatically oxidized in an electrochemical cell endowed with Pt counter electrode, Au working electrode and a SCE reference electrode in a salt bridge for 3 hours under N_2 atmosphere. The electrolysis solution is then dried and the reaction mixture is purified through column chromatography. Eluent: ethyl-acetate:hexane 1:9; as cation exchange resin sodium polystyrenesulfonate is added for electrolyte separation. One single product is obtained and characterized through 1H-NMR (Figure S 9): dimer: 9,9'-diethyl-9H,9'H-3,3'-bicarbazole.

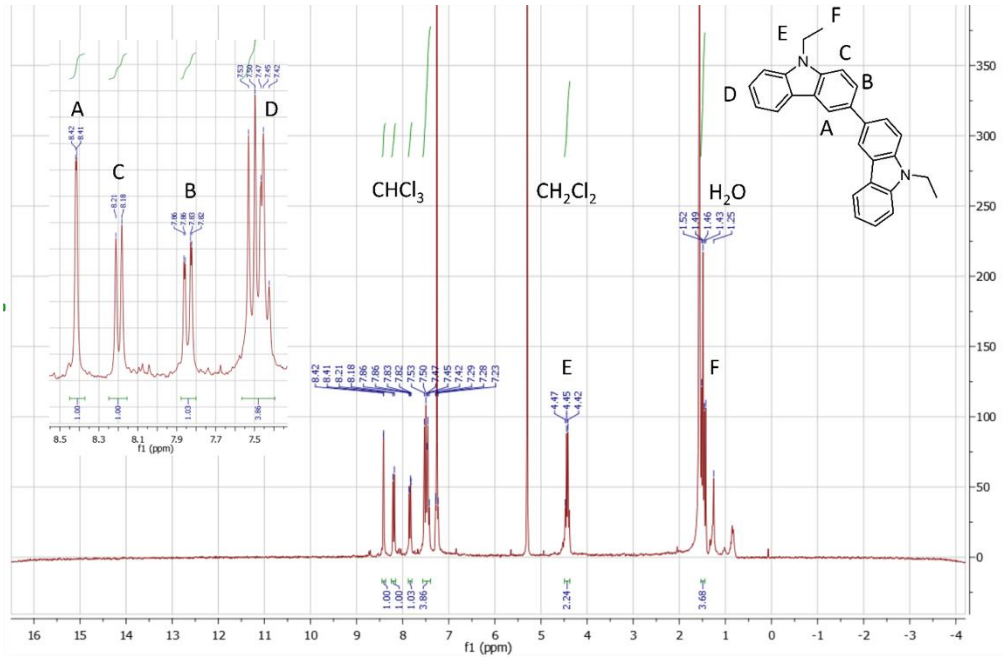

Figure S 9: 1H-NMR of electrolysis product of N-Ethylcarbazole: 9,9'-diethyl-9H,9'H-3,3'-bicarbazole.

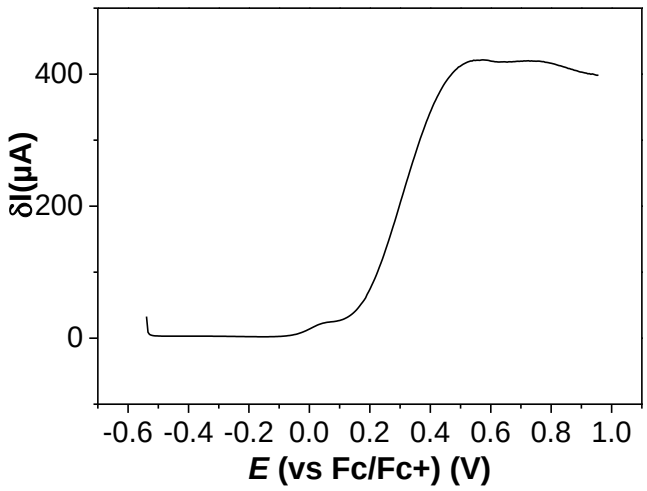

Figure S 10: Differential Pulse Voltammetry of Poly(BCbz) in CH_3CN/nNBu_4PF_6 0.1 M at 20 mV/s. dE: 25 mV.

4. *In-situ* spectroelectrochemistry and CV coupled with *in-situ* conductance

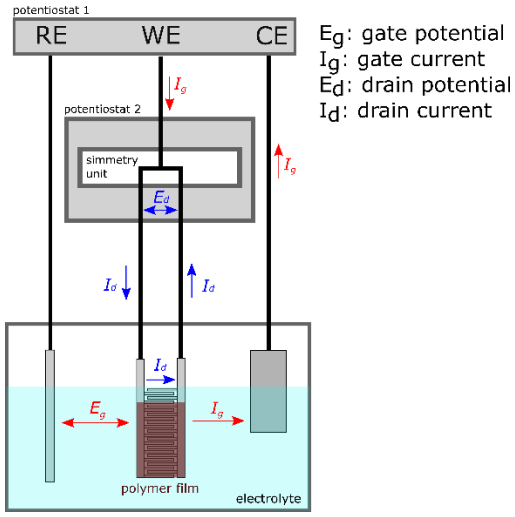

Figure S 11: Sketch of the in-situ conductance setup. Potentiostat 1 used for polarizing the WE (interdigitated electrode coated with polymer film): a gate potential (E_g) is applied between the RE and WE responsible for polymer doping and a gate current (I_g) is measured between the WE and the CE. Potentiostat 2 applies a small potential amplitude (10 mV) between the interdigitated comb (Ed) and measures the drain current (Id) between the combs from which conductance is extracted. A symmetry unit consisting of a set of resistance for current distribution to the interdigitated electrode.

Poly(TPB)

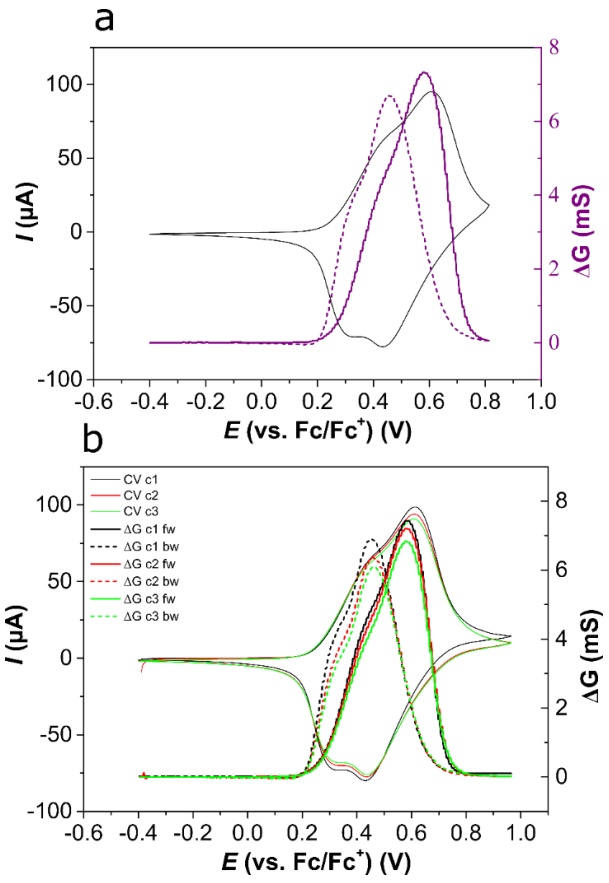

Figure S 12: In-situ conductance of Poly(TPB). (a) complete cycle from Figure 3 in main text. (b) Several cycles of same sample up to higher potentials (up to 1 V vs Fc/Fc^+). Pt-IDE 5µm; 20 mV/s in $CH_3CN/nNBu_4PF_6$ (0.1 M).

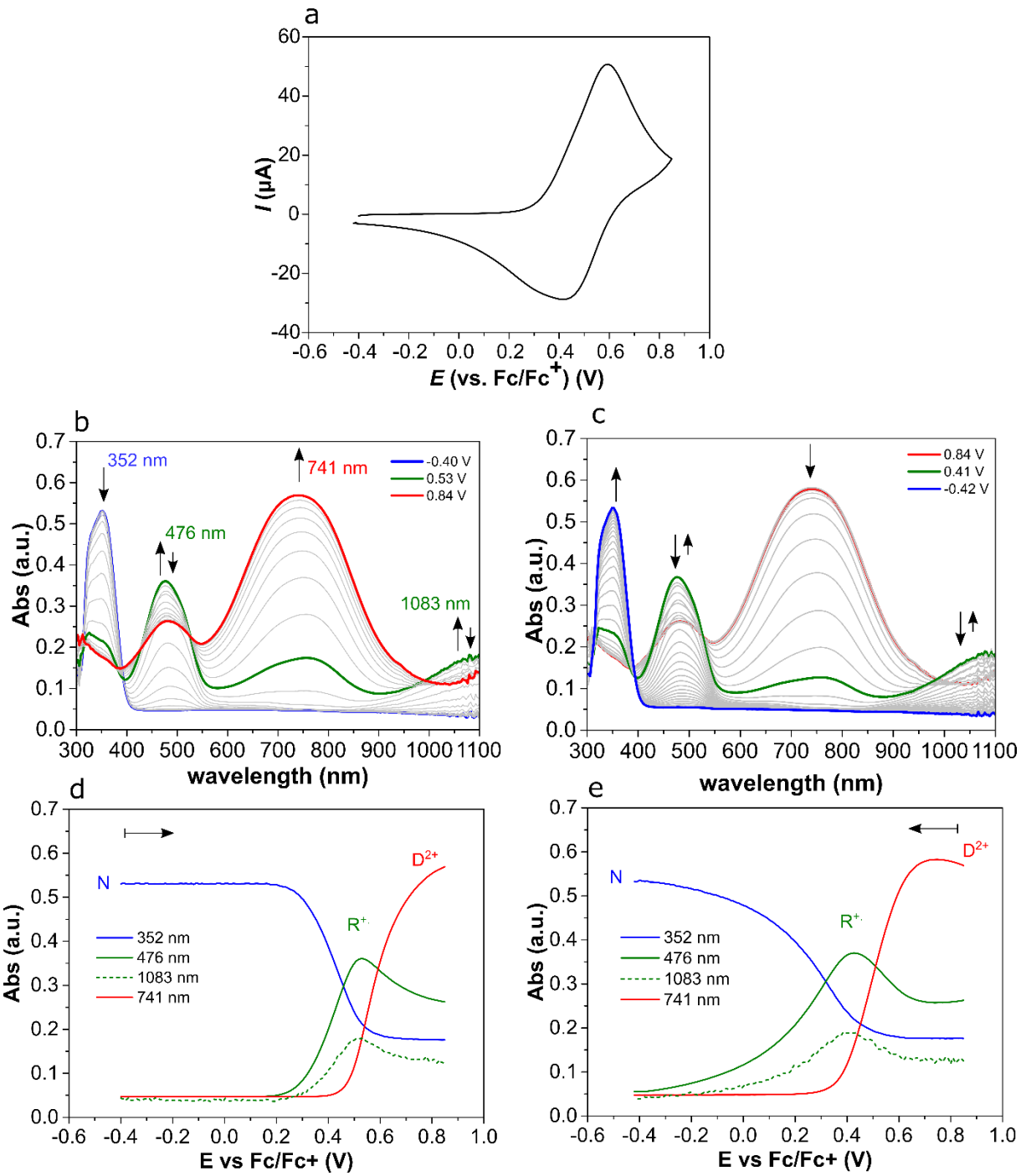

Figure S 13: In-situ spectroelectrochemistry of Poly(TPB) thin film on ITO electrode, scan-rate 20 mV/s in $CH_3CN/nNBu_4PF_6$ (0.1 M). a) CV; b) UV-Vis spectra during the forward scan; c) UV-Vis spectra during the backward scan; d) peak-evolution of representative species in the forward scan and e) peak-evolution backward scan. Neutral state indicated with blue, radical cation with green and dication with red lines.

Poly(BPhCbz)

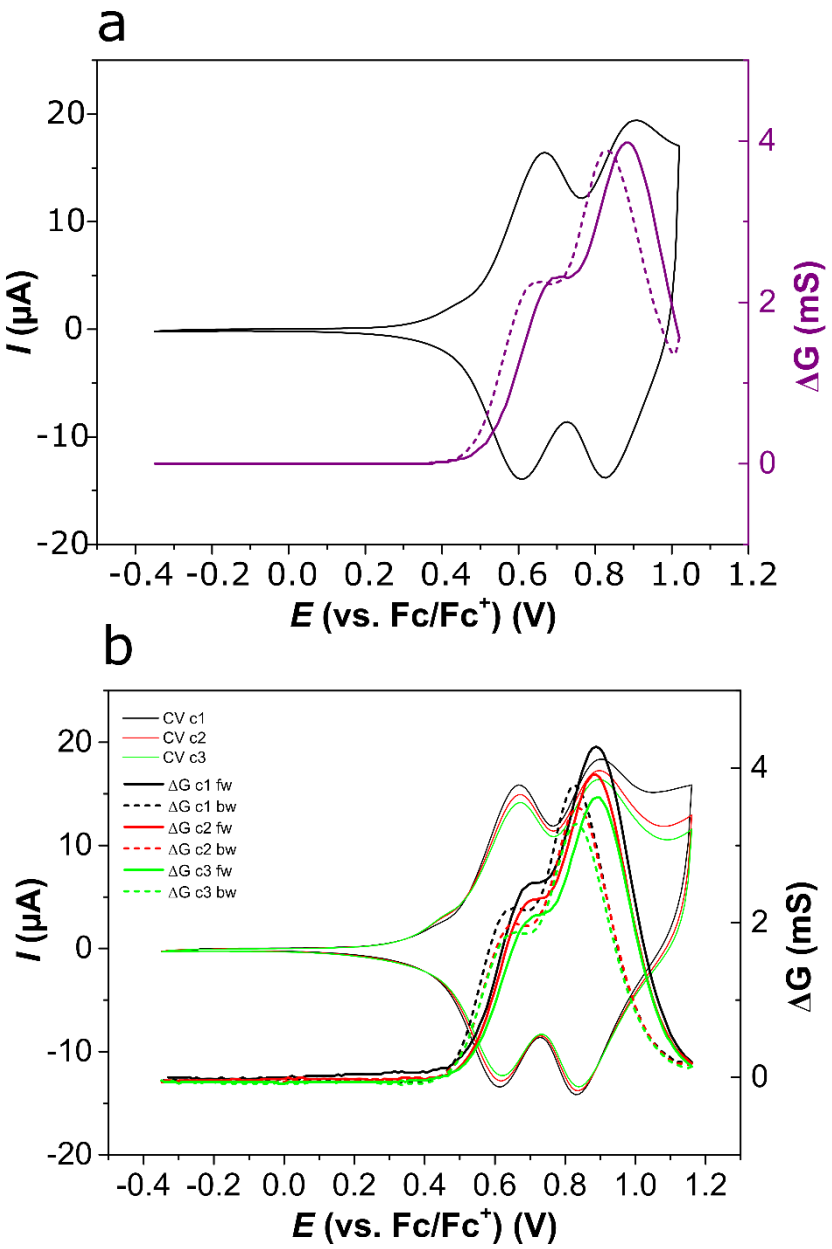

Figure S 14: In-situ conductance of Poly(BPhCbz) (a) complete cycle from Figure 4 in main text. (b) Several cycles of same sample up to higher potentials (1.2 V vs Fc/Fc$^+$). Pt-IDE 5µm; 20 mV/s s in $CH_3CN/nNBu_4PF_6$ (0.1 M).

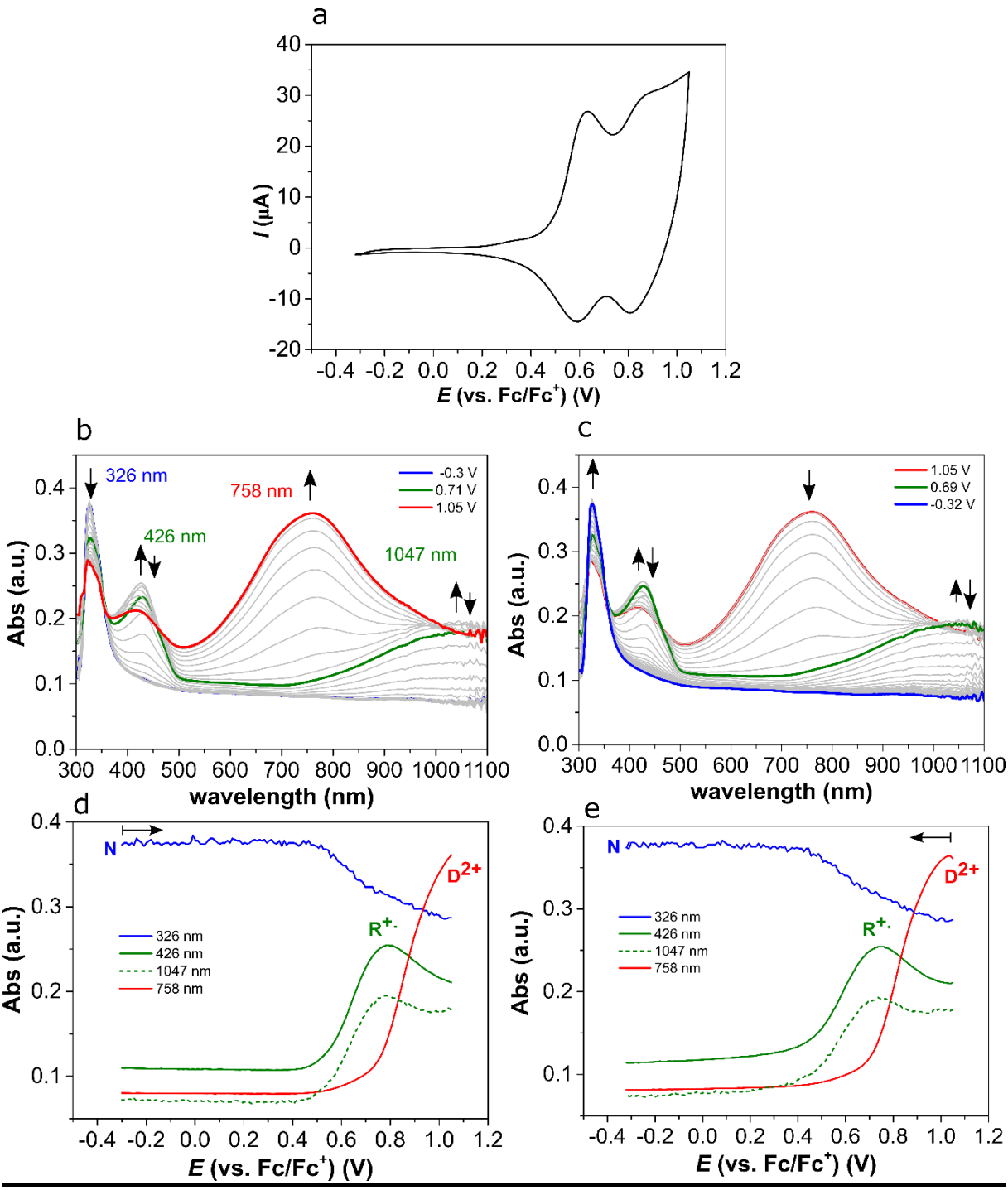

Figure S 15: In-situ spectroelectrochemistry of Poly(BPhCbz) thin film on 5µm Pt-IDE electrode, scan-rate 20 mV/s in CH_3CN/nNBu_4PF_6 0.1 M. a) CV; b) UV-Vis spectra forward scan; c) UV-Vis spectra backward scan; d) peak-evolution forward scan and e) peak-evolution backward scan. Neutral state indicated with blue, radical cation with green line and dication with red.

Poly(BCbz)

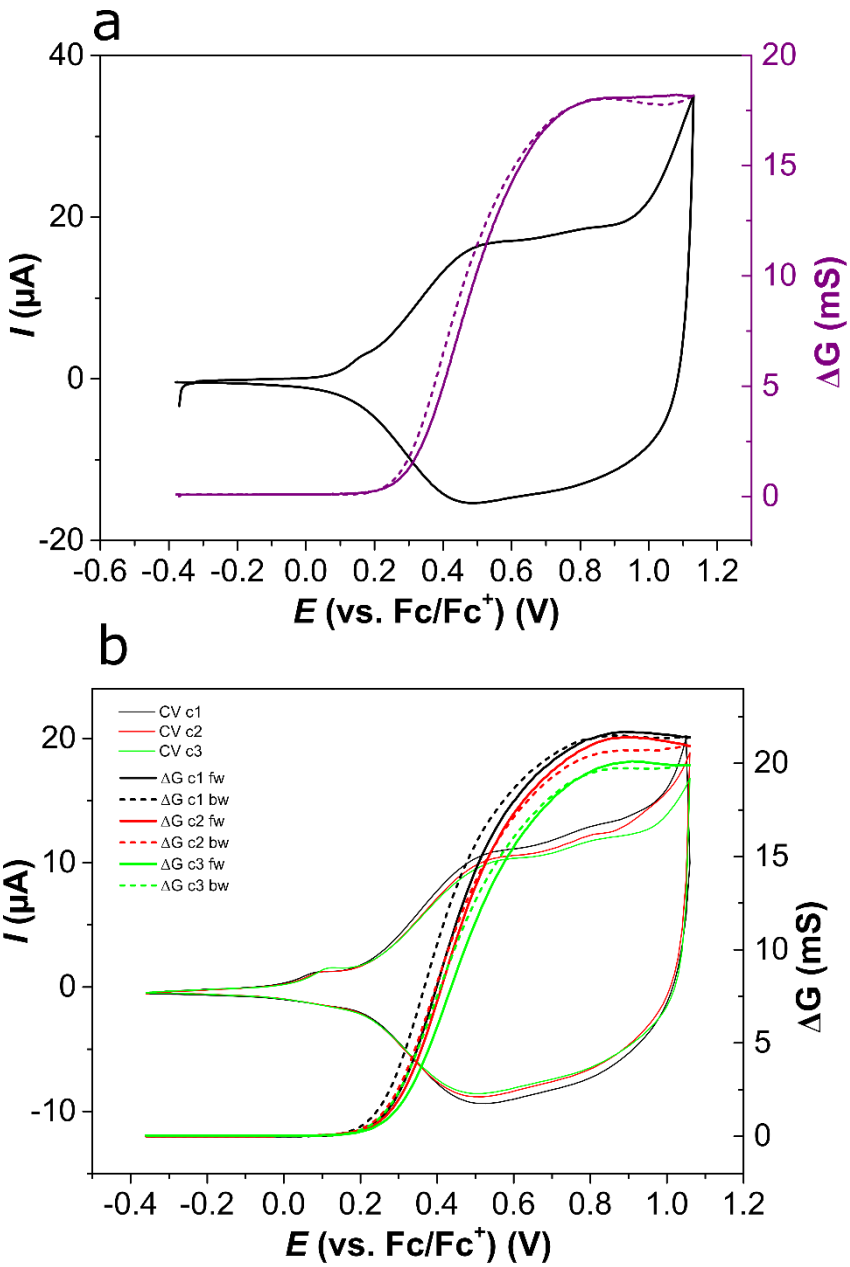

Figure S 16: In-situ conductance of Poly(BCbz) film of Figure 4 in main text cycled to 1.1 V vs Fc/Fc$^+$. (b) Several cycles (different sample). Pt-IDE 5µm; 20 mV/s s in $CH_3CN/nNBu_4PF_6$ (0.1 M).

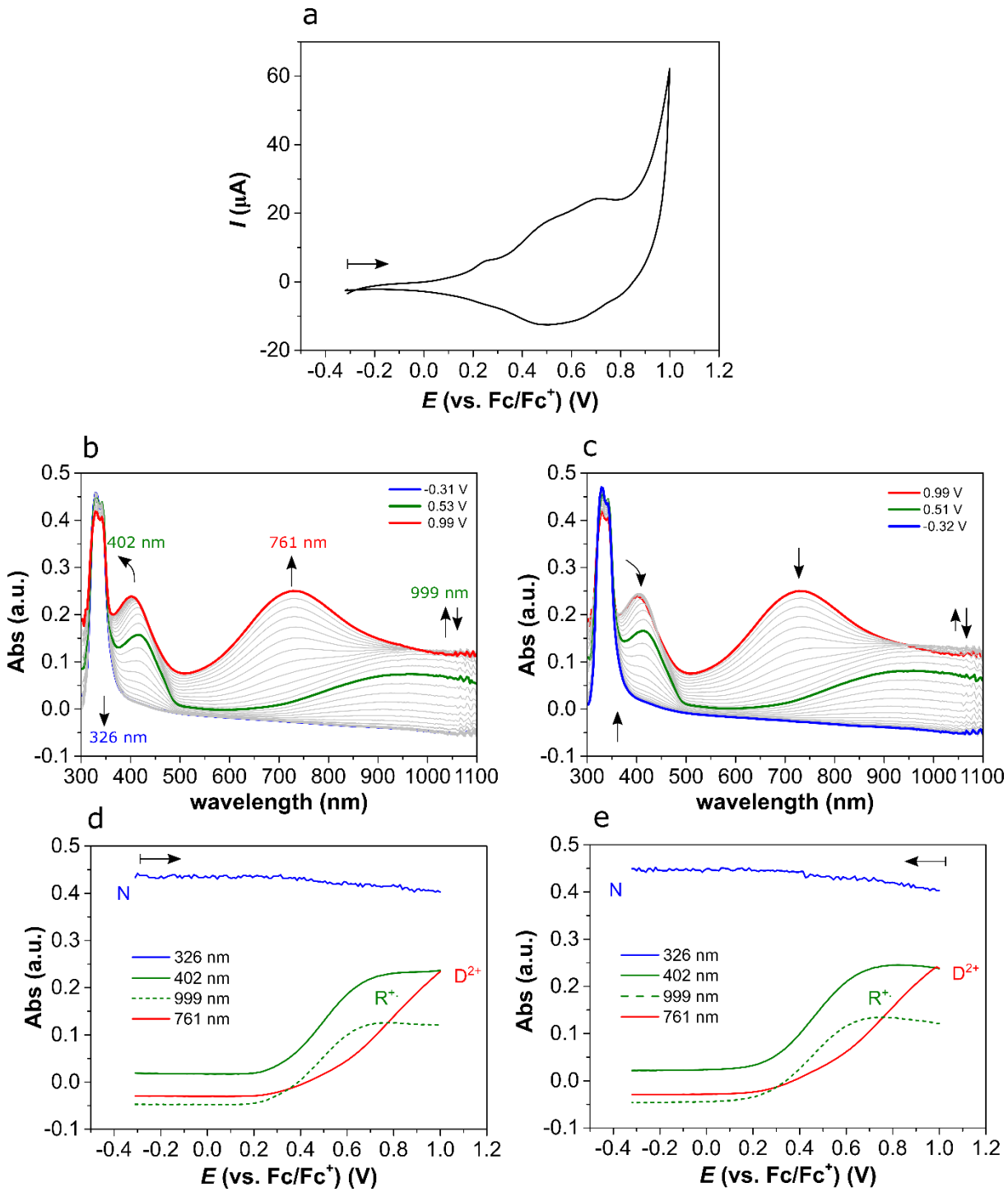

Figure S 17: In-situ spectroelectrochemistry of Poly(BCbz) thin film on 5µm Pt-IDE electrode, scan-rate 20 mV/s in CH_3CN/nNBu_4PF_6 (0.1 M). a) CV; b) UV-Vis spectra forward scan; c) UV-Vis spectra backward scan; d) peak-evolution forward scan and e) peak-evolution backward scan. Neutral state indicated with blue, radical cation with green line and dication with red.

5. DFT calculations:

The optimized geometries of TPB, BPhCbz and BCbz dimers show a planarization of the conjugated backbone upon oxidation on going from the neutral to the radical cation and dication states (see scheme 1 and Figure S 18). For the Cbz systems, the different substitution on the nitrogen atoms (i.e., phenyl vs ethyl groups) affects very slightly the molecular conformation (similar dihedral angles are predicted for BPhCbz and BCbz dimers) and the molecular electronic properties (similar HOMO and LUMO energies for the neutral states and similar SOMO energies for the cation states) are found when comparing BPhCbz and BCbz dimers, see Figures S19-S21). However, the values obtained for the TPB systems differs from those obtained for the Cbz molecules (*i.e.*, the HOMO is destabilized when compared to the Cbz dimers in agreement with its lowest first oxidation potential).

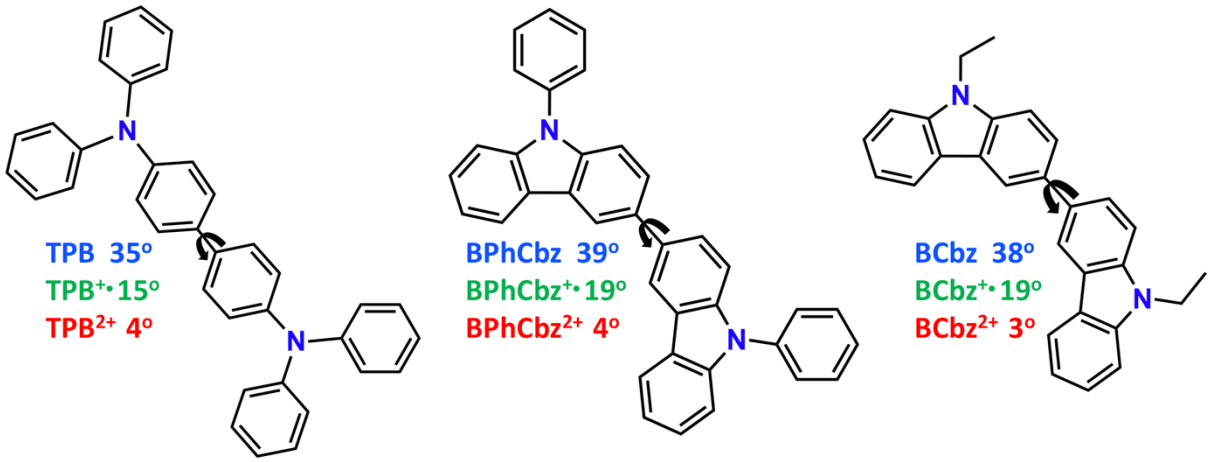

*Figure S 18: DFT-optimized dihedral angles (CAM-B3LYP/6-31G** in acetonitrile) between the TPA and Cbz units in TPB, BPhCbz and BCbz dimers, respectively.*

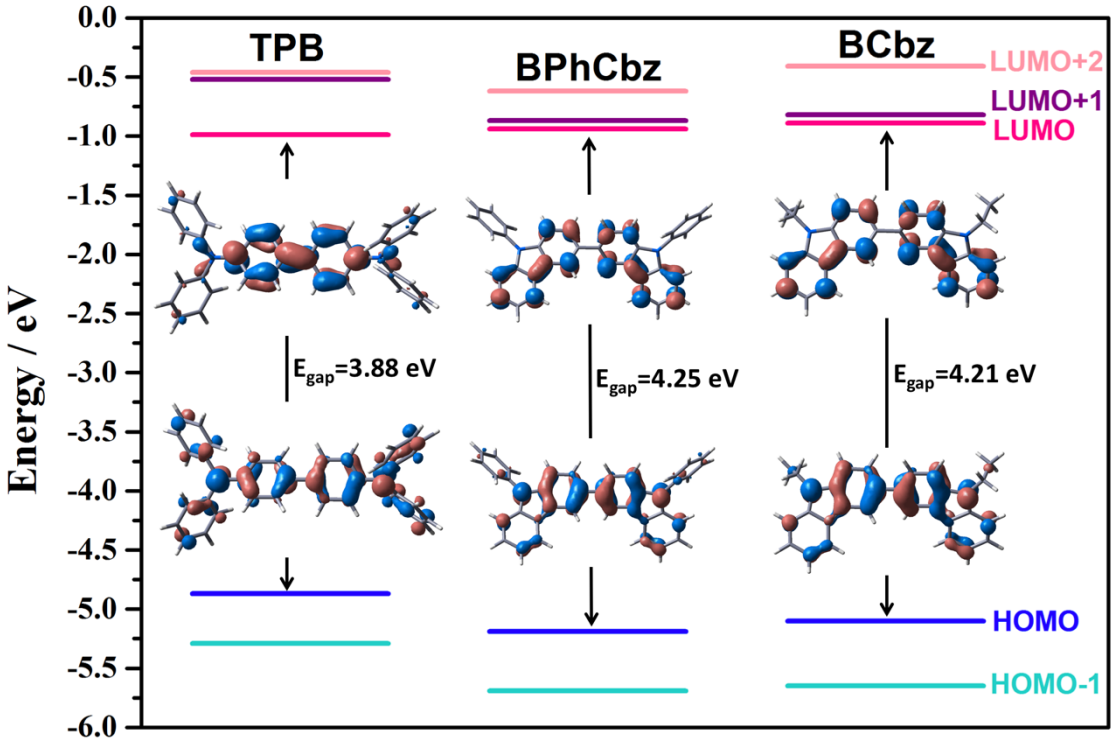

*Figure S 19: DFT-calculated frontier energy levels (B3LYP/6-31G** in acetonitrile) of TPB, BPhCbz and BCbz dimers. The HOMO and LUMO topologies are also shown.*

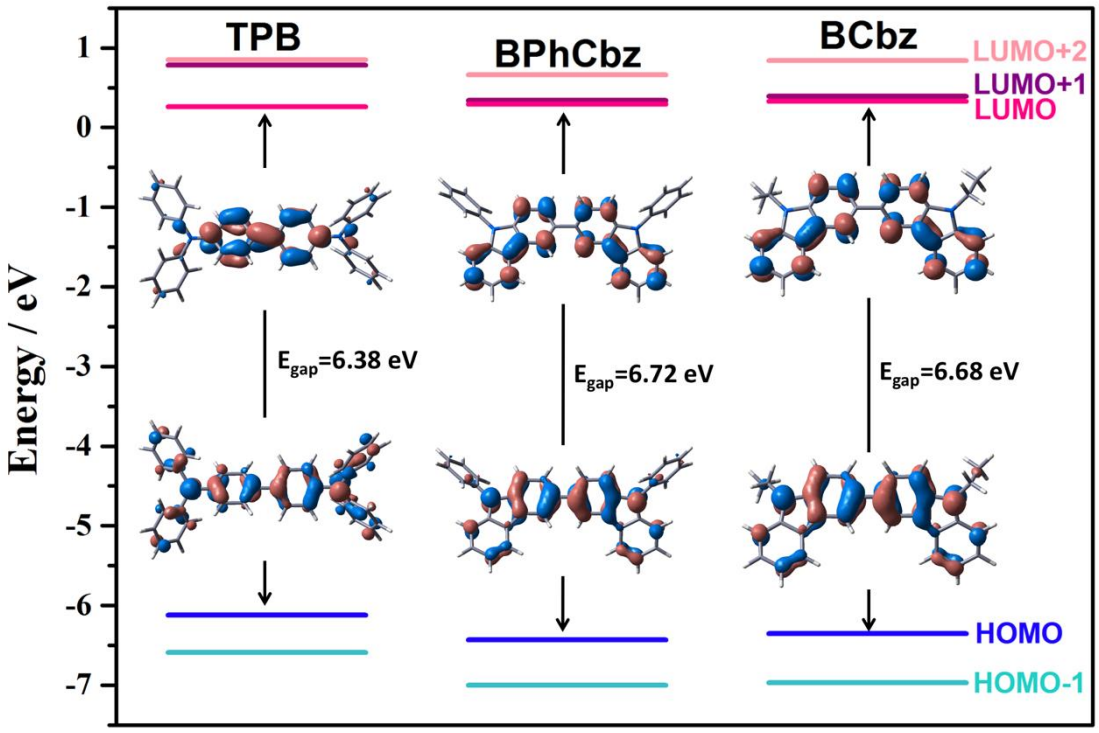

*Figure S 20: DFT-calculated frontier energy levels (CAM-B3LYP/6-31G** in acetonitrile) of TPB, BPhCbz and BCbz dimers. The HOMO and LUMO topologies are also shown.*

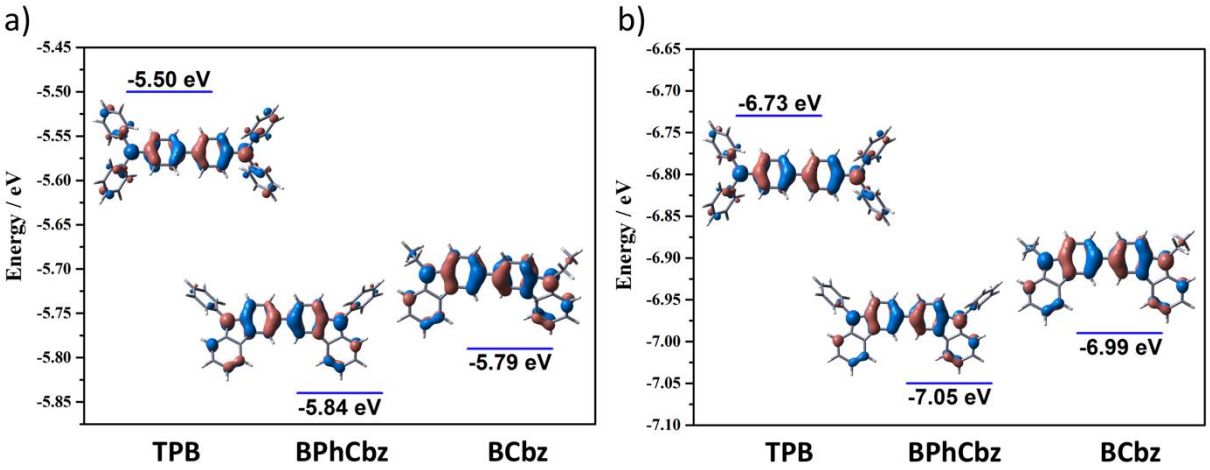

*Figure S 21: DFT-calculated SOMO energy levels and topologies of TPB, BPhCbz and BCbz dimers at the B3LYP/6-31G** (a) and CAM-B3LYP/6-31G** (b) level using acetonitrile as solvent.*

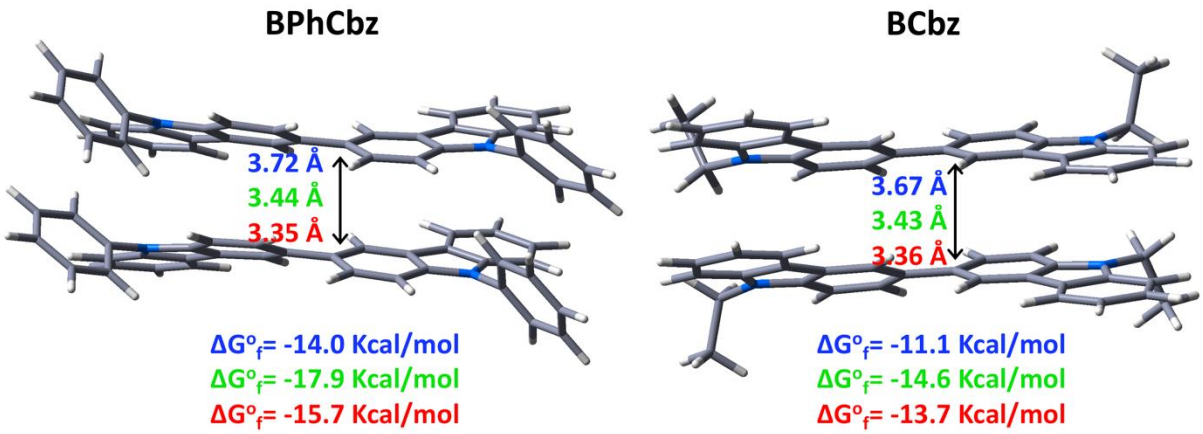

*Figure S 22: Lateral views of the DFT-computed global minimum structure pi-dimers of BPhCbz and BCbz in a syn configuration. The shortest C-C distances between the monomers and the free energy of formation values (at 298 K) calculated at the ωB97XD/6-31G** level in acetonitrile are also shown (blue, green and red values denoted the neutral, radical cation and dication states, respectively)*

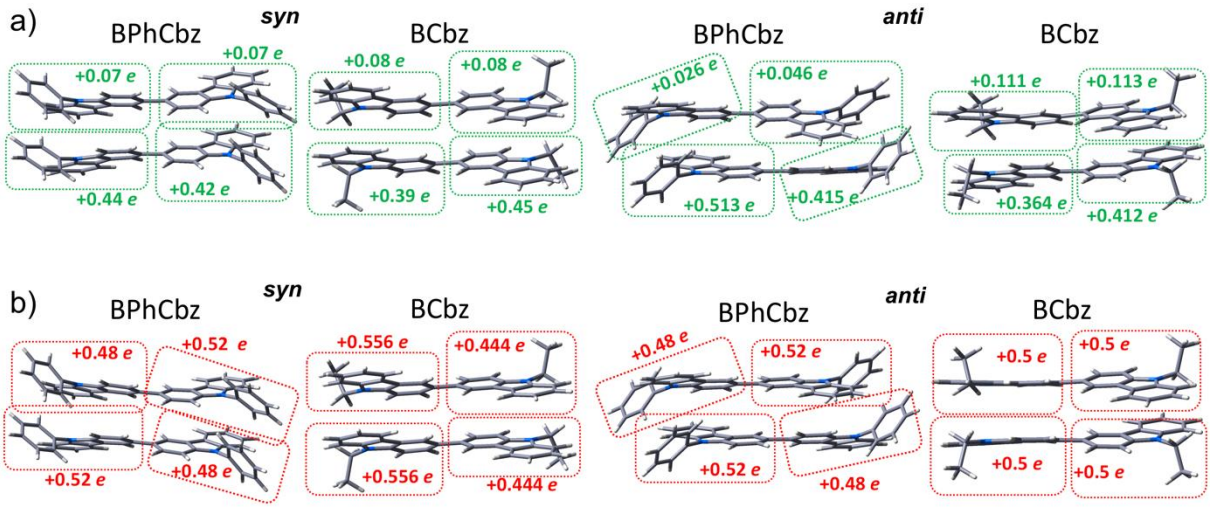

*Figure S 23: DFT-calculated Mülliken atomic charges (ωB97XD/6-31G** level in acetonitrile) on each Cbz unit of the pi-dimer aggregates of BPhCbz and BCbz in a syn (left) or anti (right) configuration for the radical cation (a) and dication (b) states.*

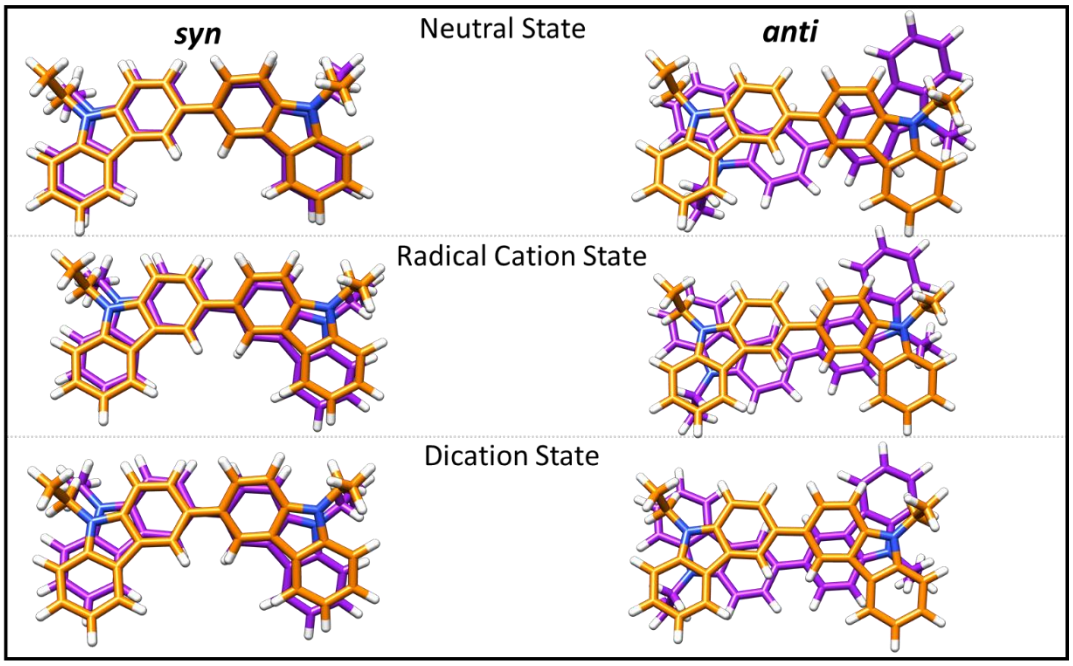

*Figure S 24: Top views of the DFT-computed (ωB97XD/6-31G** level in acetonitrile) global minimum structure pi-dimers of BCbz in syn (left) and anti (right) configurations.*

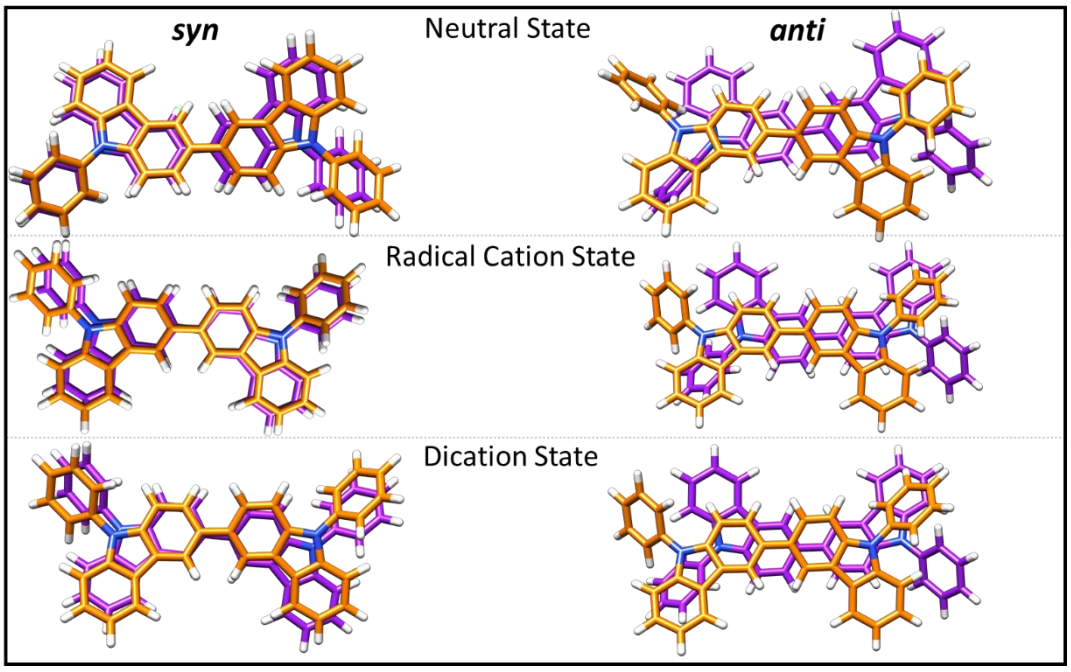

*Figure S 25: Top views of the DFT-computed (ωB97XD/6-31G** level in acetonitrile) global minimum structure pi-dimers of BPhCbz in syn (left) and anti (right) configurations.*

Computational Methods

The molecular geometries of the neutral and charged species of dimers TPB, BPhCbz and BCbz were optimized in acetonitrile (using the PCM[1] method) at the Density Functional Theory (DFT) level using the GAUSSIAN16 program.[2] Two different hybrid functionals were tested, such as the hybrid generalized gradient approximation (GGA) functional B3LYP[3] and the long-range corrected hybrid functional CAM-B3LYP[4], together with the 6-31G** basis set.[5]

Interestingly, the two B3LYP and CAM-B3LYP functionals predict the same behaviour in the description of the structural and electronic properties of TPB, BPhCbz and BCbz dimers.
On the other hand, cofacial π-dimers of BPhCbz and BCbz in *anti* and *syn* configurations were calculated at the neutral, radical cation and dication states in order to illustrate the intermolecular interactions between neighbouring redox units. In this regard, the long-range-corrected functional of Head-Gordon and coworkers ωB97XD[6] (which includes empirical dispersion) was used, together with the 6-31G** basis set.
All geometrical parameters were allowed to vary independently, and no imaginary frequencies were observed, which ensures the finding of the global minimum energy.

References

1. J. Tomasi, M. Persico, Chem. Rev. 1994, 94, 2027−2094.

2. Gaussian 16, Revision A.03, M. J. Frisch, G. W. Trucks, H. B. Schlegel, G. E. Scuseria, M. A. Robb, J. R. Cheeseman, G. Scalmani, V. Barone, G. A. Petersson, H. Nakatsuji, X. Li, M. Caricato, A. V. Marenich, J. Bloino, B. G. Janesko, R. Gomperts, B. Mennucci, H. P. Hratchian, J. V. Ortiz, A. F. Izmaylov, J. L. Sonnenberg, D. Williams-Young, F. Ding, F. Lipparini, F. Egidi, J. Goings, B. Peng, A. Petrone, T. Henderson, D. Ranasinghe, V. G. Zakrzewski, J. Gao, N. Rega, G. Zheng, W. Liang, M. Hada, M. Ehara, K. Toyota, R. Fukuda, J. Hasegawa, M. Ishida, T. Nakajima, Y. Honda, O. Kitao, H. Nakai, T. Vreven, K. Throssell, J. A. Montgomery, Jr., J. E. Peralta, F. Ogliaro, M. J. Bearpark, J. J. Heyd, E. N. Brothers, K. N. Kudin, V. N. Staroverov, T. A. Keith, R. Kobayashi, J. Normand, K. Raghavachari, A. P. Rendell, J. C. Burant, S. S. Iyengar, J. Tomasi, M. Cossi, J. M. Millam, M. Klene, C. Adamo, R. Cammi, J. W. Ochterski, R. L. Martin, K. Morokuma, O. Farkas, J. B. Foresman, and D. J. Fox, Gaussian, Inc., Wallingford CT, 2016.

3. (a) Lee, C.; Yang, W.; Parr, R. G., Development of the Colle-Salvetti correlation-energy formula into a functional of the electron density. Physical Review B 1988, 37 (2), 785-789; (b) Becke, A. D., Density-functional thermochemistry. III. The role of exact exchange. The Journal of Chemical Physics 1993, 98 (7), 5648-5652.

4. Yanai, T.; Tew, D. P.; Handy, N. C., A new hybrid exchange–correlation functional using the Coulomb-attenuating method (CAM-B3LYP). Chemical Physics Letters 2004, 393 (1), 51-57.

5. (a) Hehre, W. J.; Ditchfield, R.; Pople, J. A., Self—Consistent Molecular Orbital Methods. XII. Further Extensions of Gaussian—Type Basis Sets for Use in Molecular Orbital Studies of Organic Molecules. The Journal of Chemical Physics 1972, 56 (5), 2257-2261; (b) Francl, M. M.; Pietro, W. J.; Hehre, W. J.; Binkley, J. S.; Gordon, M. S.; DeFrees, D. J.; Pople, J. A., Self-consistent molecular orbital methods. XXIII. A polarization-type basis set for second-row elements. The Journal of Chemical Physics 1982, 77 (7), 3654-3665.

6. Chai, J.-D.; Head-Gordon, M., Long-range corrected hybrid density functionals with damped atom–atom dispersion corrections. Physical Chemistry Chemical Physics 2008, 10 (44), 6615-6620.